JBC ACCELERATED COMMUNICATION

Loss of bound zinc facilitates amyloid fibril formation of leukocyte-cell-derived chemotaxin 2 (LECT2)

Received for publication, January 11, 2021, and in revised form, February 5, 2021 Published, Papers in Press, February 20, 2021,
https://doi.org/10.1016/j.jbc.2021.100446

Jeung-Hoi Ha[1], **Ho-Chou Tu**[2], **Stephan Wilkens**[1], **and Stewart N. Loh**[1,*]

From the [1]*Department of Biochemistry and Molecular Biology, SUNY Upstate Medical University, Syracuse, New York, USA; and* [2]*Alnylam Pharmaceuticals, Cambridge, Massachusetts, USA*

Edited by Karen Fleming

Aggregation of the circulating protein leukocyte-cell-derived chemotaxin 2 (LECT2) causes amyloidosis of LECT2 (ALECT2), one of the most prevalent forms of systemic amyloidosis affecting the kidney and liver. The I40V mutation is thought to be necessary but not sufficient for ALECT2, with a second, as-yet undetermined condition being required for the disease. EM, X-ray diffraction, NMR, and fluorescence experiments demonstrate that LECT2 forms amyloid fibrils *in vitro* in the absence of other proteins. Removal of LECT2's single bound Zn^{2+} appears to be obligatory for fibril formation. Zinc-binding affinity is strongly dependent on pH: 9–13 % of LECT2 is calculated to exist in the zinc-free state over the normal pH range of blood, with this fraction rising to 80 % at pH 6.5. The I40V mutation does not alter zinc-binding affinity or kinetics but destabilizes the zinc-free conformation. These results suggest a mechanism in which loss of zinc together with the I40V mutation leads to ALECT2.

Leukocyte-cell-derived chemotaxin 2 (LECT2) is a 133-residue protein synthesized in the liver for secretion into the blood. LECT2 plays roles in immunity (1–3), inflammatory cytokine responses (4, 5), liver angiogenesis (6), and other processes (7–10). In accordance with its multifunctional status, LECT2 is associated with numerous diseases. One of these is amyloidosis of LECT2 (ALECT2). Though ALECT2 was only first reported in 2008 (11), it is now recognized as one of the most prevalent forms of systemic amyloidosis (SA) in the United States (12). SA is a class of disorders that result from misfolding of one of ∼30 circulating proteins into amyloid fibrils. These fibrils deposit in various organs—the liver and kidney in the case of ALECT2—and eventually lead to their failure (13–15).

The causes of ALECT2 are not known, but one clue comes from the genetics of the disease: all patients examined thus far are homozygous for the I40V mutation in LECT2 (12, 16, 17). I40V is a common polymorphism (16, 18), however, which has led researchers to reason that I40V is necessary but not sufficient for the disease and that a second condition is required (12, 19).

LECT2 contains three disulfide bonds and binds a single Zn^{2+} coordinated by H35, D39, and H120 with the fourth site occupied by water (Fig. 1). Zn^{2+} appears to serve a structural role rather than a catalytic one (20). Because amyloid fibrillization often proceeds from a partially unfolded conformation, it is reasonable to speculate that loss of zinc from LECT2 could lead to impairment of structure and/or stability and be the second risk factor for ALECT2. Indeed, removal of Zn^{2+} has been shown to promote aggregation of LECT2 *in vitro* (21), although no study has yet demonstrated that purified LECT2 is capable of forming amyloid fibrils on its own. V40 abuts the metal binding pocket and is adjacent to D39 (Fig. 1). Here, we determine the effect of the I40V mutation on the structure, stability, and aggregation of LECT2 in the presence and absence of zinc, in order to test the hypothesis that I40V in combination with zinc loss triggers amyloid formation.

Results

Native properties of recombinant LECT2

The protocol formulated by Tanokura *et al.* for purifying bacterially expressed LECT2 involved high-pressure denaturation and refolding (22). We developed a cleavable fusion protein system for expressing soluble LECT2 in bacteria and purifying it under exclusively native conditions, with yields >20 mg/(liter culture) of 95 % pure LECT2.

WT and I40V LECT2 eluted as monodisperse, monomeric species by size-exclusion chromatography (SEC) (Fig. S1*A* and Fig. S1*B*). We confirmed the presence of correctly-paired S-S bridges by MS (Fig. S1, *C* and *D*). Finally, to assay for activity we measured binding of LECT2 to the extracellular domain of the tyrosine kinase with Ig-like and EGF-like domains 1 (TIE1) receptor. We constructed and purified two TIE1 constructs: the 360–436 fragment originally reported by Xu *et al.* (6) and the longer 360–440 fragment that we surmised might be more representative of the TIE1 extracellular domain. We predicted that the 360–436 sequence would terminate four residues short of a full β-strand, based on homology modeling with the related TIE2 receptor (23). WT and I40V LECT2 bound with similar dissociation constants (8–12 μM) to both TIE1 constructs as determined by fluorescence anisotropy (Fig. S2). These values are higher than that reported by Xu *et al.* (0.52 μM), possibly due their different conditions (maltose

* For correspondence: Stewart N. Loh, lohs@upstate.edu.

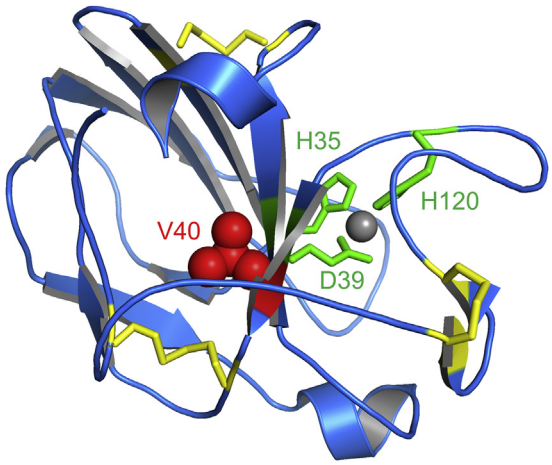

Figure 1. X-ray crystal structure of I40V LECT2. V40 (*red*) is buried and adjacent to the zinc-binding site, shown by Zn^{2+} (*gray*) and the three coordinating residues (*green*). Disulfides are in *yellow*. PDB 5B0H (20).

binding protein LECT2 fusion and surface plasmon resonance). Together, our data signify that recombinant WT and I40V LECT2 are folded and active.

Zinc-binding affinity and kinetics

The fluorescence spectrum of the single Trp residue in LECT2 shifts to higher wavelengths and increases in intensity upon zinc removal (Fig. S1*E*). We took advantage of this difference to measure K_d and the off-rate (k_{off}) of the Zn^{2+} interaction. Figure 2*A* shows that WT LECT2 binds zinc tightly (K_d = 0.79 ± 0.45 nM; Table 1) at pH 7.5, close to the normal value of the blood. Lowering pH weakens zinc binding substantially, increasing K_d to 6.6 ± 2.0 nM (pH 7.0) and 49 ± 19 nM (pH 6.5) (Fig. S3*A*). K_d values of I40V and WT LECT2 are indistinguishable within error. The 60-fold decrease in zinc affinity from pH 7.5 to pH 6.5 is not due to pH-induced unfolding or destabilization, as LECT2 is more stable at pH 6.5 than it is at pH 7.5 (Table 1). It is instead likely caused by protonation of one or more of the side chains that directly coordinate Zn^{2+}. Plotting log(K_d) versus pH provides an estimate of the number of ionizing residues participating in metal binding (Fig. S3*B*). The slope of this line is 1.78 ± 0.29 for WT LECT2 and 1.71 ± 0.13 for I40V, suggesting that two of the three zinc-binding residues, most likely H35 and H120, ionize over this pH range.

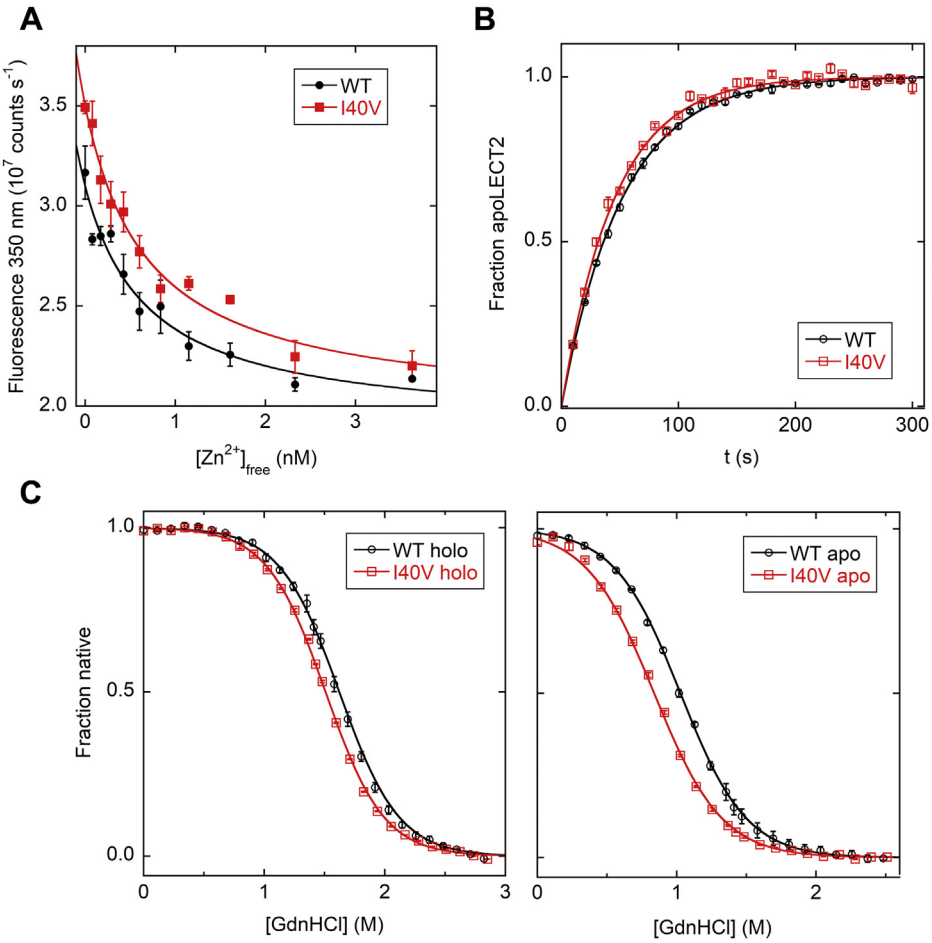

Figure 2. Zinc binding and stability of LECT2. *A*, WT and I40V LECT2 bind zinc with sub-nM K_d at pH 7.5. *B*, Zinc dissociates from WT and I40V LECT2 with half-times of 32–36 s at pH 6.5. *C*, GdnHCl denaturation finds that zinc loss destabilizes WT and I40V LECT2 (pH 7.5, 37 °C). The I40V mutation destabilizes both LECT2 and apoLECT2, but it destabilizes the latter to a greater extent. Error bars are s.d. (n = 3).

Table 1
LECT2 stability and zinc binding

LECT2	T_m (°C)	ΔG (kcal mol^{-1})	C_m (M)	K_d (nM)	k_{off} (s^{-1})
WT holo	65.77 ± 0.20[a] 72.90 ± 0.56[c]	−4.16 ± 0.10[a] −6.87 ± 0.06[c]	1.61 ± 0.04[a] 1.81 ± 0.02[c]	0.79 ± 0.45[a] 6.6 ± 2.0[b] 49 ± 19[c]	0.0098 ± 0.0021[a] 0.0194 ± 0.0005[c]
I40V holo	65.03 ± 0.21[a] 71.07 ± 1.00[c]	−3.90 ± 0.006[a] −6.69 ± 0.08[c]	1.51 ± 0.002[a] 1.76 ± 0.02[c]	0.76 ± 0.27[a] 6.0 ± 1.4[b] 40.9 ± 3.36[c]	0.0093 ± 0.0010[a] 0.0217 ± 0.0005[c]
WT apo	63.8 ± 0.096[a] 64.26 ± 1.51[c]	−2.65 ± 0.05[a] −3.92 ± 0.03[c]	1.02 ± 0.02[a] 1.32 ± 0.006[c]		
I40V apo	61.24 ± 0.28[a] 63.12 ± 1.12[c]	−2.18 ± 0.02[a] −3.70 ± 0.05[c]	0.84 ± 0.006[a] 1.24 ± 0.02[c]		

All parameters are at 37 °C except K_d (22 °C). [a]pH 7.5. [b]pH 7.0. [c]pH 6.5. Errors are s.d. (n = 3).

Our results indicate that the percentage of LECT2 in the zinc-free (apo) state is significant at typical blood pH and furthermore can shift dramatically over a physiologically accessible pH range. The total concentration of Zn^{2+} in the blood is micromolar but most is bound by albumin, leaving $[Zn^{2+}]_{free}$ ≈10 nM (24). Using this figure and the data in Table 1, the fraction of LECT2 in the apo form is calculated to be 9.0 % at pH 7.45 and 13 % at pH 7.35, the pH range considered to be normal in blood. As pH is further lowered to 7.0 and 6.5, apoLECT2 increases to 40 % and 80 %. pH can drop as low as 5.5 as fluids travel from the kidney cortical interstitium to the papilla of the kidney collecting duct (25). Since LECT2 amyloid deposits are found in the cortical interstitium in addition to kidney vasculature (16), it is possible

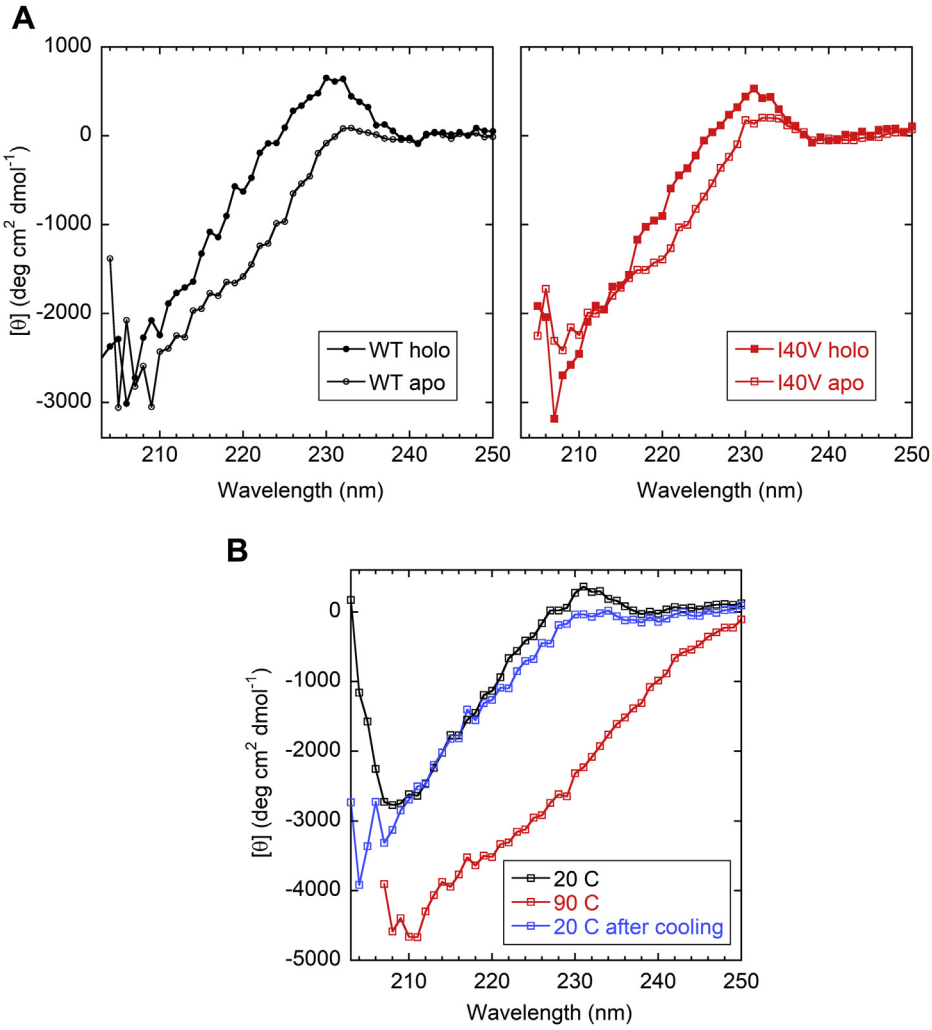

Figure 3. CD characterization of LECT2. *A*, Zinc removal slightly increases the apparent β-structure content of LECT2. *B*, The thermally denatured state of I40V LECT2 (*red*, after 15 m of heating at 90 °C) appears to increase β-structure content compared with 20 °C (*black*). The CD spectrum recovers most of its original native features upon cooling back to 20 °C (*blue*). Sample conditions are 5 μM LECT2, 20 mM Tris (pH 7.5), 0.15 M NaCl.

that LECT2 may be transiently exposed to acid conditions that cause the apo form to predominate.

Zinc dissociation rates were measured at pH 7.5 and pH 6.5 by adding excess EDTA to LECT2 and monitoring the increase in Trp fluorescence (Figs. 2*B* and S3*C*). Off-rates of WT and I40V are similar (Table 1). Zinc dissociates with a half-time of 1.2–1.5 m at pH 7.5 and 37 °C, revealing that apoLECT2 will be generated rapidly in the body once LECT2 encounters a metal chelator such as serum albumin. Off-rates increase at pH 6.5 in agreement with the equilibrium binding results (Table 1). From the thermodynamic and kinetic binding data, we conclude that there is no evidence that the I40V mutation enhances fibrillization by facilitating loss of zinc from LECT2. This finding suggests an alternate mechanism in which the I40V mutation may increase the aggregation propensity of the zinc-free protein by perturbing its structure or stability.

Stability and CD analysis of LECT2

WT and I40V LECT2 yield weak CD spectra consistent with their high content of beta sheet and loops (Fig. 3*A*) (22). An atypical positive peak at 232 nm is observed for both holo proteins, which diminishes in the apo state. Zinc removal does not unfold LECT2; rather, it increases the negative intensity of the molar ellipticity over the range of 210–235 nm, suggesting an increase in β-sheet content. Thermal denaturation produces a similar but more pronounced effect: it does not unfold LECT2 but appears to induce extensive additional beta structure (Fig. 3*B*). We used SEC to test whether CD changes observed upon zinc removal could be due to aggregation. ApoLECT2 and LECT2 eluted as monomeric peaks even after concentrating them to 210 μM at 4 °C (Fig. 1*B*).

We assessed the thermal stability of LECT2 by monitoring the change in ellipticity at 232 nm (Fig. S4*A*). Zinc-bound samples used in stability experiments (2–5 μM LECT2) contained a threefold excess of $ZnCl_2$ and a ninefold excess of iminodiacetic acid (IDA), a weak zinc chelator, to buffer $[Zn^{2+}]_{free}$ at 6–8 μM. Denaturation was ∼90 % reversible (Fig. 3*B*). At pH 7.5, removing zinc destabilizes WT LECT2 as evidenced by a 2 °C lower melting temperature (T_m) of the apo protein (Table 1). The I40V mutation does not appreciably change thermal stability of LECT2 (ΔT_m <1 °C), but it significantly destabilizes apoLECT2 (ΔT_m = -2.6 °C). The main effect of lowering pH to 6.5 is to stabilize both holo and apoLECT2, especially the former (ΔT_m = 7.1 °C for WT). The I40V mutation destabilizes the holo and apo proteins to similar extents (ΔT_m = 1.2–1.3 °C).

As an additional probe of stability, we performed guanidinium hydrochloride (GdnHCl) denaturation experiments using Trp fluorescence to report on conformation (Fig. 2*C* and S4*B*). Unfolding was again reversible in all cases, lending confidence in the reported values of folding free energy (ΔG_{fold}) and midpoint of denaturation (C_m). We judge changes in stability by ΔC_m rather than $\Delta\Delta G_{fold}$ because C_m is more accurately determined than ΔG_{fold}. In agreement with the thermal melting data, the I40V mutation destabilizes apoLECT2 (ΔC_m = -0.29 M) more so than the holo protein (ΔC_m = -0.10 M) at pH 7.5 (Table 1). Decreasing pH to 6.5 globally stabilizes LECT2. Together, the thermal and GdnHCl denaturation data show that: (i) zinc removal destabilizes LECT2 and appears to increase β-sheet content, and (ii) the I40V mutation destabilizes both holo and apo LECT2 with this effect being more pronounced on the latter.

NMR analysis of holo and apo LECT2

We recorded ^{15}N heteronuclear single-quantum correlation (HSQC) NMR spectra to gain insight into how loss of zinc affects LECT2 structure. In agreement with the HSQC data of Zheng *et al.* (22), we observed that WT LECT2 produces sharp, resolved cross peaks indicative of a well-folded protein (Fig. 4*A*). The I40V mutation causes ∼12 peaks to shift slightly, consistent with minor perturbation of structure.

In contrast to LECT2, apoLECT2 HSQC spectra exhibit a mixture of sharp and broad cross peaks and substantial collapse of chemical shift dispersion (Fig. 4*B*). These effects were not due to aggregation: SEC verified that apoLECT2 samples were monomeric prior to NMR data collection (Fig. S1*B*). Zinc loss appears to disrupt the tertiary structure of LECT2 and impart structural heterogeneity with conformational exchange occurring over a range of time scales. This result is surprising given the similarity in CD spectra and stabilities of the apo and holo proteins. Our HSQC spectrum of WT apoLECT2 also stands in contrast to that of Zheng *et al.* (22), which was similar to their spectrum of WT LECT2. The likely reason is that Zheng *et al.* generated apoLECT2 by employing IDA instead of EDTA to chelate zinc. Using the K_d values of $IDA{\cdot}Zn^{2+}$ (3.2×10^{-5} M) and $(IDA)_2{\cdot}Zn^{2+}$ (4.8×10^{-9} M^2) (26) and the data in Table 1, only 18 % of LECT2 is calculated to exist in the apo form under conditions of their NMR experiment (0.2 mM LECT2, 1 mM IDA, pH 7.0).

Structural characterization of amyloid

As an initial screen for aggregation, we performed centrifugation assays to explore a range of holo and apo LECT2 concentrations (5–20 μM) and incubation conditions, all at 37 °C and pH 7.5. Two factors proved to be essential for aggregation. The first condition was vigorous agitation. In its absence, LECT2 and apoLECT2 remained soluble and monomeric for weeks. Shaking the samples at 200 rpm in an orbital shaker was also insufficient to cause precipitation. Only by mechanically agitating the LECT2 solutions, either by magnetic stir bar (stirring method) or by shaking in the presence of silica beads (bead shake method), were we able to observe precipitation within 24–72 h. The second essential condition was removal of Zn^{2+} (*vide infra*).

We performed X-ray fiber diffraction to probe whether precipitated apoLECT2 contains amyloid structure. ApoLECT2 samples were stirred for 72 h and centrifuged. Amyloid fibrils are characterized by a strong 4.8 Å reflection corresponding to the H-bonding distance between β-strands, and a more diffuse 8–12 Å ring arising from the intersheet spacing (27, 28); 4.8 Å and 8.3 Å reflections were detected for WT and I40V apoLECT2, as well as a 5.8 Å ring that has been reported

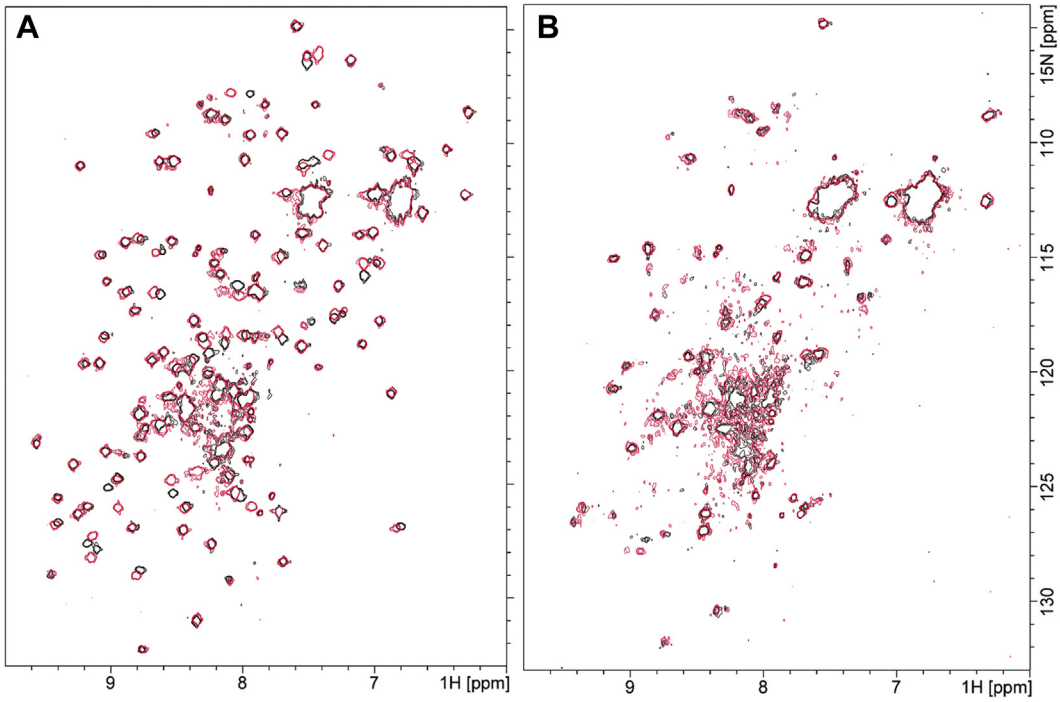

Figure 4. 800 MHz ^{15}N-HSQC NMR spectra of LECT2 (*A*) and apoLECT2 (*B*) show pronounced chemical shift changes upon zinc removal. WT and I40V LECT2 are indicated in *black* and *red*, respectively. Sample conditions are 0.2 mM LECT2, 20 mM sodium phosphate (pH 6.8), 0.15 M NaCl, 25 °C.

for other amyloid fibrils (27) (Fig. S5). Fiber diffraction data could not be collected for LECT2 without first removing zinc by EDTA, as these proteins did not precipitate.

To further confirm amyloid fibrils and characterize their morphology, we used negative stain transmission EM to image apoLECT2 during stirring. At 48 h, the predominant species were soluble, globular oligomers (<20 nm diameter) and short, individual fibrils that were present in the supernatant after centrifugation (Fig. 5*A*). No pellets were visible. A rapid transformation took place over the next 24 h in which most of the protein had precipitated and very little was detected in the supernatant. EM analysis of the insoluble fractions revealed extensive amyloid fibrils (Fig. 5*B*). WT and I40V appeared similar at both time points. Unlike the individual filaments that are frequently reported for other amyloid-forming proteins such as Alzheimer Aβ peptide (28,29), LECT2 fibrils tended to associate with each other and sometimes formed large "islands" that resembled amyloid deposits isolated from ALECT2 patient kidneys (c.f. Fig. 2*F* of reference (16)). Our data show for the first time that purified, recombinant LECT2 can form amyloid fibrils in the absence of other proteins and identify zinc loss and agitation as two critical factors for fibrillization.

Effect of the I40V mutation on aggregation

To compare aggregation propensities of WT and I40V LECT2, we employed the bead shake method in the presence of thioflavin T (ThT), a dye that fluoresces more strongly upon binding to amyloid fibrils. The negative controls (WT and I40V LECT2 containing excess $ZnCl_2$/IDA) failed to show ThT binding after extended shaking times, confirming that zinc removal is required for aggregation (Fig. 5*C*). In the presence of EDTA, apoLECT2 followed sigmoidal nucleation-growth-saturation kinetics typical of amyloid formation. The more aggressive bead shake technique resulted in shorter lag phases compared with those observed in EM and X-ray experiments. WT apoLECT2 yielded reproducible curves from experimental replicates (performed using samples prepared independently from the same frozen protein stocks) as well as technical replicates (aliquots of the same experimental replicate, agitated in different wells of the microtiter plate) (Fig. 5*C*). I40V apoLECT2 also exhibited sigmoidal kinetics but with more variability. The lag times of I40V and WT were similar, but the growth phase of I40V could be less or more pronounced than that of WT, leading to lower or higher apparent saturation levels. We observed this variability among experimental and technical replicates alike, implying that aggregation of I40V apoLECT2 is inherently more chaotic than that of WT apoLECT2.

ThT binds most strongly to mature amyloid fibrils, but it can also interact with protofilaments and soluble oligomers (30). To investigate whether the variable ThT signal of I40V apoLECT2 could be caused by different populations of these species, we shook 12 samples in beads for 24 h, removed aliquots for measuring total ThT fluorescence (ThT_{total}), then centrifuged the remaining solution, and measured the ThT fluorescence of the soluble fraction ($ThT_{soluble}$) as well as the concentration of soluble protein in the supernatant (by means of the bicinchoninic acid (BCA) assay). The supernatants exhibited a large range of protein concentrations (45–89 % of the starting amount), consistent with the variability seen in Figure 5*C*, and only background levels of $ThT_{soluble}$ (Fig. S6).

The latter finding indicates that ThT binds only to insoluble apoLECT2 and not to the soluble oligomers observed by EM. No correlation was observed, however, between the fraction of insoluble protein (given by 1 – (fraction soluble protein)) and ThT_{total} (Fig. S6). These results together suggest that there are at least two forms of aggregated apoLECT2: one that binds ThT and one that does not. The fluctuation in ThT_{total} values may be caused by apoLECT2 partitioning to one form or the other, with I40V exhibiting more pronounced variability than WT.

Discussion

Prior to this work, it had not been established whether LECT2 forms amyloid fibrils on its own or requires other factors, nor had any hypotheses been tested regarding a second-hit condition for ALECT2. A recent study of LECT2 fragments found that the 52–58 and 79–88 peptides formed amyloid fibrils (31). These residues comprise the third and fifth β-strands of the β-barrel (Fig. 1). The zinc-binding residues D39 and H120 reside in the first and second strands. It is possible that loss of the bridging zinc ion weakens the interaction between strands 1 and 2 and that the destabilizing effect propagates down the β-sheet to expose the amyloidogenic sequences in strands 3 and 5. Consistent with this view, apoLECT2 is less thermodynamically stable than LECT2, and NMR spectra show loss of tertiary structure upon zinc removal.

The extreme dependence of zinc affinity on pH suggests a potential route of ALECT2 pathology. Unlike many proteins that tetrahedrally coordinate zinc *via* four amino acids including 2–4 Cys, LECT2 employs two His, one Asp, and one water. The pK_a value of His is lower than that of Cys and is in the physiological range. LECT2 is especially vulnerable to pH-induced zinc loss. Our data predict that a significant fraction of LECT2 (9–13 %) is already in the apo state at normal blood pH and that apoLECT2 can become the dominant form under mildly acidic conditions. Aggregation rates depend critically on the concentration of nucleating species, so it seems reasonable to speculate that ALECT2 may be driven in part by abnormally low pH in the blood, kidney, or the liver cells that produce LECT2.

Zinc deficiency is another condition that can result in improper demetallation of zinc-binding proteins. Most ALECT2 patients are older adults and, in the United States, ∼90 % are Hispanic (15, 32, 33). The Third National Health and Nutrition Examination Survey (34) found that total daily zinc intake is significantly lower for 18+ year adult Hispanics in the United States compared with whites, and this gap progressively widens in the 51–70 years and 71+ years age groups. At least some of the discrepancy appears to be due to the higher use of zinc-containing supplements by whites.

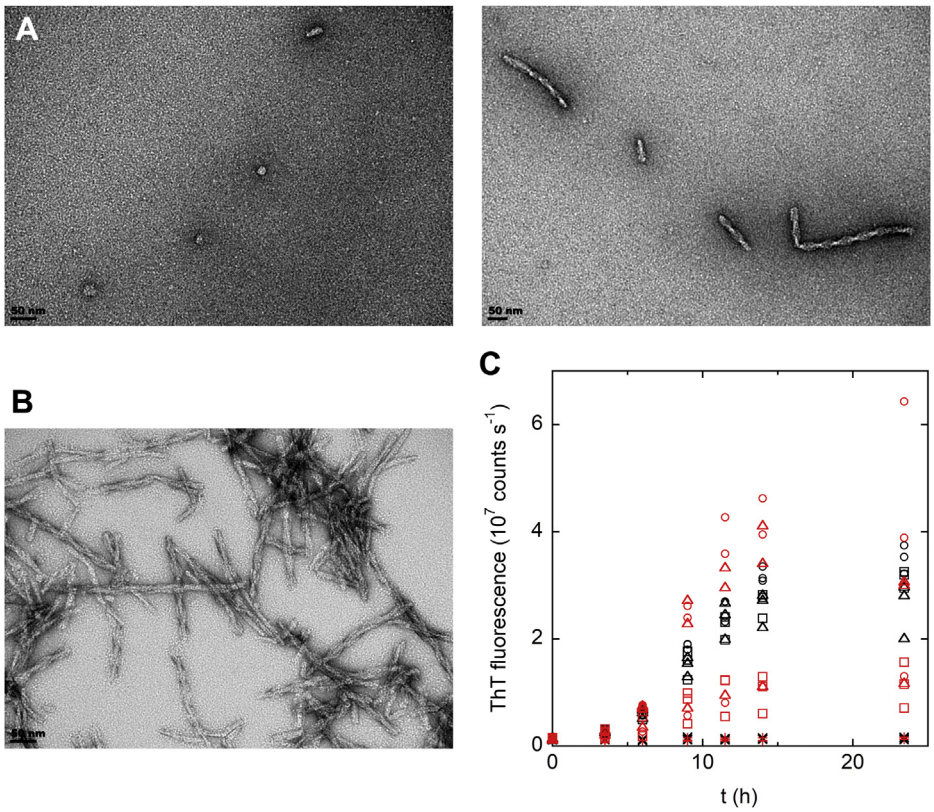

Figure 5. Aggregation of apoLECT2 characterized by EM and ThT. *A*, EM images of I40V apoLECT2 recorded after 48 h of stirring (pH 6.5, 37 °C) reveal mostly small, globular aggregates and short filaments, both detected in the soluble fraction. *B*, After 72 h of stirring, I40V apoLECT2 forms insoluble amyloid fibrils that further associate into clusters. Images of WT apoLECT2 appeared similar. Scale bars are 50 nm. *C*, Aggregation kinetics of apoLECT2 (pH 6.5, 37 °C) monitored by ThT fluorescence show greater variability for I40V (*red*) compared with WT (*black*). *Circles*, *squares*, and *triangles* indicate independent experiments (with three technical replicates per time point). Negative controls are denoted by x and +.

While the role of zinc in ALECT2 remains speculative, the known risk factor for ALECT2 is homozygosity of the I40V allele. Our studies reveal that the main effect of the I40V mutation is to destabilize LECT2 when it is in the apo form. Thus, the I40V mutation does not facilitate zinc loss, but instead may affect the aggregation propensity of apoLECT2 by increasing the conformational heterogeneity of the partially unfolded ensemble. ThT experiments provide some support for this scenario: I40V apoLECT2 exhibits more chaotic behavior compared with WT apoLECT2, with aggregation kinetics of I40V appearing faster or slower in seemingly random fashion. Further structural and dynamic studies of apoLECT2 are needed to resolve this question.

High metal concentrations have long been suspected to contribute to disease by facilitating improper binding to proteins. Aggregates of proteins such as Alzheimer Aβ peptide, α-synuclein, and amylin have been found with nonnative metal ions bound to them including zinc and copper (35, 36). Even a small molar excess of free zinc drives misfolding of p53 (37). The opposite is true for LECT2: adding extra zinc protects against aggregation, and removing it strongly facilitates amyloidogenesis. In the latter respect, apoLECT2 is reminiscent of the zinc-deficient form of superoxide dismutase (38). As with many other aggregating protein systems, vigorous agitation greatly accelerates fibrillogenesis of apoLECT2. Pressing questions remain as to whether mechanical disruption of LECT2 structure is required for its aggregation *in vivo*, and in what form this disruption may manifest in the body.

Experimental procedures

Full gene construction, protein expression, and purification protocols are included in SI Methods. Amino acid sequences of proteins used in this study are shown in Fig. S8. Experimental buffers are listed in Fig. S9.

Zinc and TIE1 binding

LECT2 was purified with ∼1 equivalent of bound Zn^{2+} as determined by incubating it with (2-pyridylazo)resorcinol (ε_{492} = 71,500 M^{-1} cm^{-1}) (39) in 6 M GdnHCl. ApoLECT2 was generated by incubating LECT2 with 0.1 mM EDTA for at least 24 h at room temperature.

For zinc-affinity measurements, $[Zn^{2+}]_{free}$ was fixed at the indicated values by mixing 1.6 mM $ZnCl_2$ and 2.0 mM EGTA in buffer 1, performing serial dilutions, and calculating $[Zn^{2+}]_{free}$ using the MaxChelator software (https://somapp.ucdmc.ucdavis.edu/pharmacology/bers/maxchelator/). Trp fluorescence spectra were recorded using a SpectaMax i3x plate reader (Molecular Devices) with excitation at 275 nm. Fluorescence intensity at 350 nm was fit to the one-site binding equation to determine zinc K_d values. Zinc k_{off} was determined by mixing LECT2 with 0.1 mM EDTA and fitting the increase in Trp fluorescence at 340 nm to a one-exponential function.

TIE1 was labeled at its N-terminal amine by treating it with a 1.5-fold excess of fluorescein NHS ester (Thermo Fisher) and removing unreacted label (DG-10 column, BioRad). TIE1 (50 nM) was mixed with the indicated concentrations of LECT2 in buffer 2, and fluorescence anisotropy was recorded on the plate reader. Anisotropy data were fit to the one-site binding equation to determine K_d values.

Protein stability

GdnHCl denaturation experiments were performed by mixing 2 μM LECT2 (in buffer 3) with 2 μM LECT2 in 4 M GdnHCl at various ratios. Trp fluorescence was recorded using a FluoroMax 4 fluorimeter (Horiba) with excitation at 280 nm. Fluorescence intensities from 320 to 325 nm were summed and fit to the linear extrapolation equation (LEE) (40) to determine ΔG, C_m, and *m*-values. WT and I40V data were fit using a single, pooled *m*-value (2.84 ± 0.07 and 3.67 ± 0.11 for LECT2 at pH 7.5 and pH 6.5, respectively, and 2.54 ± 0.08 and 2.88 ± 0.08 for apoLECT2 at pH 7.5 and pH 6.5, respectively, in units of kcal mol^{-1} M^{-1}). CD scans and thermal melts were recorded on a Model 420 spectropolarimeter (Aviv Biomedical) with heating steps of 1 °C/2 m. The data were fit to the LEE to obtain apparent T_m values.

ThT fluorescence

Samples consisted of 10 μM LECT2, 20 μM ThT containing 0.1 mM EDTA (or 30 μM $ZnCl_2$, 90 μM IDA for negative controls), in buffer 4. In total, 150 μl aliquots were placed in 96-well round-bottom, black, polystyrene plates (Corning) with six 1-mm diameter polystyrene beads (BioSpec) per well. Plates were shaken on a vortexer (37 °C) and scanned with excitation at 410 nm and emission at 490 nm. BCA assays were performed following the manufacturer's protocol (Thermo Fisher).

NMR, EM, X-ray, and MS

^{15}N-labeled LECT2 samples in buffer 5 were concentrated and run through a Superdex S200I column (Cytiva) to ensure no aggregation had taken place, at which point monomeric protein was transferred to the NMR spectrometer. Data were acquired on an Avance III 800 MHz NMR spectrometer equipped with a cryogenic probe (Bruker Daltonics).

Aggregated protein samples for EM and X-ray diffraction experiments were prepared by stirring 0.5 ml of 10–20 μM LECT2 in buffer 1 and 0.1 mM EDTA with a 3 x 10 mm spin bar (SP Bel-Art) in a 1.5 ml microfuge tube (37 °C). Samples were centrifuged at 16,100×*g* for 15 m. For EM experiments, the pellets were resuspended in 20–50 μl buffer 1, placed on carbon-coated copper grids, washed with water, and stained with 1 % $C_4H_6O_6U$. Samples for X-ray diffraction were resuspended in 5 μl water, then placed between two capillaries as described (41). EM and X-ray data were collected on a JEM-1400 electron microscope (JEOL) with Orius 832 CCD (Gatan) at 200,000X magnification and an Excalibur PX Ultra diffractometer with Onyx CCD detector (Oxford Instruments).

For MS analysis, I40V LECT2 was digested with MS grade trypsin (Promega). One-half of the sample was reduced with dithiothreitol, then alkylated with iodoacetamide. Data were

acquired on an Orbitrap XL mass spectrometer (Thermo Fisher). MS data from the two samples were compared to identify the locations of the disulfide bonds.

Data availability

All data are contained within the article and supporting information.

Supporting information—This article contains supporting information.

Acknowledgments—We thank Dr Edward Berry for assistance with the X-ray diffraction experiments. This work was funded by an award from Alnylam Pharmaceuticals.

Author contributions—J.-H. H., H.-C. T, and S. N. L. conceived of the study. J.-H. H. and S. N. L. designed the experiments. J.-H. H., S. W., and S. N. L. performed the experiments and analyzed the data. S. N. L wrote the original draft. J.-H. H. and S. W. edited the draft and made revisions.

Funding and additional information—S. W. is supported by NIH grant GM058600.

Conflict of interest—The authors declare that they have no conflicts of interest with the contents of this article.

Abbreviations—The abbreviations used are: ALECT2, amyloidosis of leukocyte-cell-derived chemotaxin 2; apoLECT2, leukocyte-cell-derived chemotaxin 2 lacking its single bound zinc ion; BCA, bicinchoninic assay; C_m, midpoint of chemical denaturation; GdnHCl, guanidine hydrochloride; HSQC, heteronuclear single-quantum correlation; IDA, iminodiacetic acid; K_d, equilibrium dissociation constant of zinc binding; k_{off}, zinc dissociation rate; LECT2, leukocyte-cell-derived chemotaxin 2; SA, systemic amyloidosis; SEC, size-exclusion chromatography; ThT, thioflavin T; TIE, tyrosine kinase with immunoglobulin-like and EGF-like domains; T_m, midpoint of thermal denaturation.

References

1. Lu, X.-J., Chen, J., Yu, C. H., Shi, Y. H., He, Y. Q., Zhang, R. C., Huang, Z. A., Lv, J. N., Zhang, S., and Xu, L. (2013) LECT2 protects mice against bacterial sepsis by activating macrophages via the CD209a receptor. *J. Exp. Med.* **210**, 5–13
2. Wang, Z., Lu, J., Li, C., Li, Q., and Pang, Y. (2018) Characterization of the LECT2 gene and its protective effects against microbial infection via large lymphocytes in Lampetra japonica. *Dev. Comp. Immunol.* **79**, 75–85
3. Shen, H. X., Li, L., Chen, Q., He, Y. Q., Yu, C. H., Chu, C. Q., Lu, X. J., and Chen, J. (2016) LECT2 association with macrophage-mediated killing of Helicobacter pylori by activating NF-κB and nitric oxide production. *Genet. Mol. Res.* **15**, 1–14
4. Hwang, H.-J., Jung, T. W., Hong, H. C., Seo, J. A., Kim, S. G., Kim, N. H., Choi, K. M., Choi, D. S., Baik, S. H., and Yoo, H. J. (2015) LECT2 induces atherosclerotic inflammatory reaction via CD209 receptor-mediated JNK phosphorylation in human endothelial cells. *Metab. Clin. Exp.* **64**, 1175–1182
5. Ando, K., Kato, H., Kotani, T., Ozaki, M., Arimura, Y., and Yagi, J. (2012) Plasma leukocyte cell-derived chemotaxin 2 is associated with the severity of systemic inflammation in patients with sepsis. *Microbiol. Immunol.* **56**, 708–718
6. Xu, M., Xu, H. H., Lin, Y., Sun, X., Wang, L. J., Fang, Z. P., Su, X. H., Liang, X. J., Hu, Y., Liu, Z. M., Cheng, Y., Wei, Y., Li, J., Li, L., Liu, H. J., *et al.* (2019) LECT2, a Ligand for Tie1, plays a Crucial role in liver Fibrogenesis. *Cell* **178**, 1478–1492.e20
7. Lu, X.-J., Chen, Q., Rong, Y. J., Yang, G. J., Li, C. H., Xu, N. Y., Yu, C. H., Wang, H. Y., Zhang, S., Shi, Y. H., and Chen, J. (2016) LECT2 drives haematopoietic stem cell expansion and mobilization via regulating the macrophages and osteolineage cells. *Nat. Commun.* **7**, 12719
8. Chen, C.-K., Yu, W. H., Cheng, T. Y., Chen, M. W., Su, C. Y., Yang, Y. C., Kuo, T. C., Lin, M. T., Huang, Y. C., Hsiao, M., Hua, K. T., Hung, M. C., and Kuo, M. L. (2016) Inhibition of VEGF165/VEGFR2-dependent signaling by LECT2 suppresses hepatocellular carcinoma angiogenesis. *Sci. Rep.* **6**, 31398
9. Chen, C.-K., Yang, C. Y., Hua, K. T., Ho, M. C., Johansson, G., Jeng, Y. M., Chen, C. N., Chen, M. W., Lee, W. J., Su, J. L., Lai, T. C., Chou, C. C., Ho, B. C., Chang, C. F., Lee, P. H., *et al.* (2014) Leukocyte cell-derived chemotaxin 2 antagonizes MET receptor activation to suppress hepatocellular carcinoma vascular invasion by protein tyrosine phosphatase 1B recruitment. *Hepatology* **59**, 974–985
10. L'Hermitte, A., Pham, S., Cadoux, M., Couchy, G., Caruso, S., Anson, M., Crain-Denoyelle, A. M., Celton-Morizur, S., Yamagoe, S., Zucman-Rossi, J., Desdouets, C., and Couty, J. P. (2019) Lect2 controls inflammatory Monocytes to Constrain the growth and progression of hepatocellular carcinoma. *Hepatology* **69**, 160–178
11. Benson, M. D., James, S., Scott, K., Liepnieks, J. J., and Kluve-Beckerman, B. (2008) Leukocyte chemotactic factor 2: A novel renal amyloid protein. *Kidney Int.* **74**, 218–222
12. Dogan, A. (2017) Amyloidosis: Insights from Proteomics. *Annu. Rev. Pathol.* **12**, 277–304
13. Larsen, C. P., Walker, P. D., Weiss, D. T., and Solomon, A. (2010) Prevalence and morphology of leukocyte chemotactic factor 2-associated amyloid in renal biopsies. *Kidney Int.* **77**, 816–819
14. Said, S. M., Sethi, S., Valeri, A. M., Leung, N., Cornell, L. D., Fidler, M. E., Herrera Hernandez, L., Vrana, J. A., Theis, J. D., Quint, P. S., Dogan, A., and Nasr, S. H. (2013) Renal amyloidosis: Origin and clinicopathologic correlations of 474 recent cases. *Clin. J. Am. Soc. Nephrol.* **8**, 1515–1523
15. Mereuta, O. M., Theis, J. D., Vrana, J. A., Law, M. E., Grogg, K. L., Dasari, S., Chandan, V. S., Wu, T. T., Jimenez-Zepeda, V. H., Fonseca, R., Dispenzieri, A., Kurtin, P. J., and Dogan, A. (2014) Leukocyte cell-derived chemotaxin 2 (LECT2)-associated amyloidosis is a frequent cause of hepatic amyloidosis in the United States. *Blood* **123**, 1479–1482
16. Nasr, S. H., Dogan, A., and Larsen, C. P. (2015) Leukocyte cell-derived chemotaxin 2-associated amyloidosis: A recently recognized disease with Distinct clinicopathologic Characteristics. *Clin. J. Am. Soc. Nephrol.* **10**, 2084–2093
17. Yamagoe, S., Kameoka, Y., Hashimoto, K., Mizuno, S., and Suzuki, K. (1998) Molecular cloning, structural characterization, and chromosomal mapping of the human LECT2 gene. *Genomics.* **48**, 324–329
18. Kameoka, Y., Yamagoe, S., Hatano, Y., Kasama, T., and Suzuki, K. (2000) Val58Ile polymorphism of the neutrophil chemoattractant LECT2 and rheumatoid arthritis in the Japanese population. *Arthritis Rheum.* **43**, 1419–1420
19. Slowik, V., and Apte, U. (2017) Leukocyte cell-derived chemotaxin-2: It's role in Pathophysiology and Future in Clinical Medicine. *Clin. Transl. Sci.* **10**, 249–259
20. Zheng, H., Miyakawa, T., Sawano, Y., Asano, A., Okumura, A., Yamagoe, S., and Tanokura, M. (2016) Crystal structure of human leukocyte cell-derived chemotaxin 2 (LECT2) reveals a Mechanistic Basis of functional Evolution in a Mammalian protein with an M23 Metalloendopeptidase fold. *J. Biol. Chem.* **291**, 17133–17142
21. Okumura, A., Suzuki, T., Miyatake, H., Okabe, T., Hashimoto, Y., Miyakawa, T., Zheng, H., Unoki-Kubota, H., Ohno, H., Dohmae, N., Kaburagi, Y., Miyazaki, Y., Tanokura, M., and Yamagoe, S. (2013) Leukocyte cell-derived chemotaxin 2 is a zinc-binding protein. *FEBS Lett.* **587**, 404–409
22. Zheng, H., Miyakawa, T., Sawano, Y., Yamagoe, S., and Tanokura, M. (2013) Expression, high-pressure refolding and purification of human leukocyte cell-derived chemotaxin 2 (LECT2). *Protein Expr. Purif.* **88**, 221–229
23. Barton, W. A., Tzvetkova-Robev, D., Miranda, E. P., Kolev, M. V., Rajashankar, K. R., Himanen, J. P., and Nikolov, D. B. (2006) Crystal structures

of the Tie2 receptor ectodomain and the angiopoietin-2–Tie2 complex. *Nat. Struct. Mol. Biol.* **13**, 524–532
24. Blindauer, C. A., Harvey, I., Bunyan, K. E., Stewart, A. J., Sleep, D., Harrison, D. J., Berezenko, S., and Sadler, P. J. (2009) Structure, properties, and engineering of the major zinc binding site on human albumin. *J. Biol. Chem.* **284**, 23116–23124
25. Zalyapin, E. A., Bouley, R., Hasler, U., Vilardaga, J. P., Lin, H. Y., Brown, D., and Ausiello, D. A. (2008) Effects of the renal medullary pH and ionic environment on vasopressin binding and signaling. *Kidney Int.* **74**, 1557–1567
26. Krężel, A., and Maret, W. (2016) The biological inorganic chemistry of zinc ions. *Arch. Biochem. Biophys.* **611**, 3–19
27. Sunde, M., Serpell, L. C., Bartlam, M., Fraser, P. E., Pepys, M. B., and Blake, C. C. (1997) Common core structure of amyloid fibrils by synchrotron X-ray diffraction. *J. Mol. Biol.* **273**, 729–739
28. Serpell, L. C. (2000) Alzheimer's amyloid fibrils: Structure and assembly. *Biochim. Biophys. Acta* **1502**, 16–30
29. Roychaudhuri, R., Yang, M., Hoshi, M. M., and Teplow, D. B. (2009) Amyloid β-protein assembly and Alzheimer disease. *J. Biol. Chem.* **284**, 4749–4753
30. Gade Malmos, K., Blancas-Mejia, L. M., Weber, B., Buchner, J., Ramirez-Alvarado, M., Naiki, H., and Otzen, D. (2017) ThT 101: A primer on the use of thioflavin T to investigate amyloid formation. *Amyloid* **24**, 1–16
31. Tsiolaki, P. L., Nasi, G. I., Baltoumas, F. A., Fishman, S., Tu, H. C., and Iconomidou, V. A. (2019) Delving into the amyloidogenic core of human leukocyte chemotactic factor 2. *J. Struct. Biol.* **207**, 260–269
32. Larsen, C. P., Beggs, M. L., Wilson, J. D., and Lathrop, S. L. (2016) Prevalence and organ distribution of leukocyte chemotactic factor 2 amyloidosis (ALECT2) among decedents in New Mexico. *Amyloid* **23**, 119–123
33. Said, S. M., Sethi, S., Valeri, A. M., Chang, A., Nast, C. C., Krahl, L., Molloy, P., Barry, M., Fidler, M. E., Cornell, L. D., Leung, N., Vrana, J. A., Theis, J. D., Dogan, A., and Nasr, S. H. (2014) Characterization and outcomes of renal leukocyte chemotactic factor 2-associated amyloidosis. *Kidney Int.* **86**, 370–377
34. Briefel, R. R., Bialostosky, K., Kennedy-Stephenson, J., McDowell, M. A., Ervin, R. B., and Wright, J. D. (2000) Zinc intake of the U.S. Population: Findings from the third National Health and Nutrition Examination Survey, 1988–1994. *J. Nutr.* **130**, 1367S–1373S
35. Atrián-Blasco, E., Gonzalez, P., Santoro, A., Alies, B., Faller, P., and Hureau, C. (2018) Cu and Zn coordination to amyloid peptides: From fascinating chemistry to debated pathological relevance. *Coord. Chem. Rev.* **371**, 38–55
36. Lei, P., Ayton, S., and Bush, A. I. (2021) The essential elements of Alzheimer's disease. *J. Biol. Chem.* **296**, 100105
37. Yu, X., Blanden, A. R., Narayanan, S., Jayakumar, L., Lubin, D., Augeri, D., Kimball, S. D., Loh, S. N., and Carpizo, D. R. (2014) Small molecule restoration of wildtype structure and function of mutant p53 using a novel zinc-metallochaperone based mechanism. *Oncotarget* **5**, 8879–8892
38. Oztug Durer, Z. A., Cohlberg, J. A., Dinh, P., Padua, S., Ehrenclou, K., Downes, S., Tan, J. K., Nakano, Y., Bowman, C. J., Hoskins, J. L., Kwon, C., Mason, A. Z., Rodriguez, J. A., Doucette, P. A., Shaw, B. F., *et al.* (2009) Loss of metal ions, disulfide Reduction and mutations related to Familial ALS promote formation of amyloid-like aggregates from superoxide dismutase. *PLoS ONE* **4**, e5004
39. Kocyła, A., Pomorski, A., and Krężel, A. (2015) Molar absorption coefficients and stability constants of metal complexes of 4-(2-pyridylazo) resorcinol (PAR): Revisiting common chelating probe for the study of metalloproteins. *J. Inorg. Biochem.* **152**, 82–92
40. Santoro, M. M., and Bolen, D. W. (1988) Unfolding free energy changes determined by the linear extrapolation method. 1. Unfolding of phenylmethanesulfonyl alpha chymotrypsin using different denaturants. *Biochemistry* **27**, 8063–8068
41. Morris, K. L., and Serpell, L. C. (2012) X-ray Fibre diffraction studies of amyloid fibrils. In: Sigurdsson, E. M., Calero, M., Gasset, M., eds. *Amyloid Proteins: Methods and Protocols*, Humana Press, New York, NY: 121–135